Construction and Building Materials 116 (2016) 159–168

Contents lists available at ScienceDirect

Construction and Building Materials

journal homepage: www.elsevier.com/locate/conbuildmat

Field assessment of oxidative aging in asphalt concrete pavements with unknown acoustic properties

Megan E. McGovern [a], William G. Buttlar [b], Henrique Reis [a,*]

[a] Department of Industrial and Enterprise Systems Engineering, University of Illinois at Urbana-Champaign, 104 S. Mathews Avenue, Urbana, IL 61801, United States
[b] Department of Civil and Environmental Engineering, University of Illinois at Urbana-Champaign, 205 N. Mathews Avenue, Urbana, IL 61801, United States

HIGHLIGHTS

- Nonlinear ultrasonics effective to evaluate aging in asphalt concrete pavements.
- Technique is truly nondestructive and easy to operate.
- Technique only requires access to pavement surface for aging evaluation.
- Oxidative aging evolution is plotted in a two-dimensional space.
- Approach has potential to evaluate rejuvenator efficiency.

ARTICLE INFO

Article history:
Received 28 May 2015
Received in revised form 15 April 2016
Accepted 26 April 2016
Available online 4 May 2016

Keywords:
Asphalt concrete
Pavements
Oxidative aging
Field testing
Longitudinal subsurface waves
Non-collinear wave mixing
Nonlinear ultrasonics

ABSTRACT

Because in the field asphalt concrete acoustic properties (*i.e.*, velocities and corresponding attenuations) are unknown, a modified version of the non-collinear wave mixing method is proposed to evaluate oxidative aging levels. Longitudinal transducers mounted on angle wedges are employed to launch subsurface dilatational waves to allow evaluation when there is only access to one side of the asphalt concrete pavement. For the mixture used, one fixed incident angle was found, which is suitable for the range of oven-aged asphalt concrete specimens, *i.e.*, 0–36 h. Theoretical explanation and experimental evidence supporting the validity of the proposed approach is presented.

1. Introduction

Thermal, block and top-down cracking in asphalt concrete (AC) pavements are major forms of distress that are highly detrimental to pavement quality and service life once initiated. Repeated exposure to environmental conditions accelerate the formation, growth, and coalescence of micro-flaws, which results in the development of damaging macro-cracks. Exposure to oxygen is one of the main contributors to micro-crack formation in asphalt concrete (AC) pavements, where the micro-flaw population is directly related to the amount of oxidative aging of the AC. Once degradation has progressed to the point where micro-cracks are present, the pavement is susceptible to further damage as moisture and oxygen can infiltrate further into its depth [1,2]. As a result, millions of dollars are spent annually in repair and maintenance of AC pavements. It is more cost effective to frequently provide maintenance on pavements that are still in "fair" condition than it is to defer maintenance until the pavement deterioration has reached a "poor" state; consequently, determining the proper time for repair and maintenance is a critical issue [3,4]. Visual inspection alone is not always adequate to evaluate the state-of-damage of a pavement, mainly because damage may not be visible despite the fact that diffuse micro-flaw populations may already exist in abundance. Furthermore, even if these diffuse flaw populations do not yet exist, the binder state-of-oxidative aging is such that diffuse flaw populations are just about to develop, mainly because of the increasing loss of binder viscoelastic relaxation capabilities and adhesive properties. Currently, there is no practical method to in-situ nondestructively evaluate the level of oxidative-aging of pavements before major deterioration has taken place. Clearly, there

* Corresponding author.
E-mail addresses: meg.e.mcg@gmail.com (M.E. McGovern), buttlar@illinois.edu (W.G. Buttlar), h-reis@illinois.edu (H. Reis).

http://dx.doi.org/10.1016/j.conbuildmat.2016.04.117
0950-0618/

exists a need for a practical, easy-to-use method to nondestructively assess the level of oxidative-aging of AC pavements.

Asphalt concrete belongs to a class of materials named mesoscopic materials that are made of brick and mortar; in asphalt concrete the brick are the aggregates and the mortar is the binder [5,6]. In this class of materials, most of the deformation is concentrated in the mortar, which leads to these material to exhibit nonlinear response, even before any micro-flaws develop. Masad et al. [7–9] found that asphalt binders exhibit both linear and nonlinear viscoelastic behavior and the level of nonlinearity increases with stress or strain levels. Masad et al. [7–9] also observed that the average binder strain is 9-to-12 times the mixture strain, and that the maximum binder strain can be as high as 90 times the mixture strain. The nonlinear response of binders and mixtures was also studied by Delgadillo [10]. As aging progresses, the asphalt concrete increases in stiffness and loses adhesive properties. Initially, the increase in stiffness dominates the phenomenon; however, with continued increase in oxidation the loss of the binder's adhesive properties starts to dominate the phenomenon, which leads to the development of diffuse flaw populations. As these diffuse flaw population's increase in size with higher levels of oxidative aging, the asphalt concrete also increases its nonlinear response.

When an ultrasonic wave is transmitted through a material that exhibits nonlinear behavior, it also displays nonlinear behavior characterized by the nonlinear acoustic wave equation [11,12]. This nonlinear behavior can manifest itself in the form of the presence of higher order harmonics, or in the case when more than one wave intercepts at an angle, they may interact and produce a third wave of different mode, polarization and propagating in a different direction. When two waves interact to produce a third wave, *i.e.*, wave-mixing, the efficiency at which the third wave is generated is related to the presence of local material nonlinearities (*e.g.*, micro-flaws), whose characteristic lengths may be orders of magnitude smaller than the wavelengths traditionally used in linear ultrasonic nondestructive evaluation. This third wave is referred to as the "nonlinear scattered wave," and in order to be generated, the interaction between the two primary waves must meet resonance and polarization conditions [13–18].

In a previous study [19], it was shown that non-collinear wave mixing of dilatational subsurface waves can be used to estimate the nonlinearities in AC. Due to oxidative aging, most of the damage occurs in the binder, which with increasing levels of oxidative-aging becomes increasingly stiffer, less relaxant and less adhesive. The material nonlinearities increase with oxidative-aging, *i.e.*, the rate of damage accumulation increases. Therefore, characterizing these nonlinearities provides a tool to assess the level of oxidative-aging of the AC. In AC pavements, there is only access to one side, *i.e.*, the pavement surface; therefore, in order to be truly non-destructive, the measurements should only be taken from the surface by employing transducers mounted on variable angle wedges. As shown in Fig. 1, the incident angle of the wedges should be set to an angle close to the first critically refracted angle so that a majority of the wave energy propagates near and parallel to the surface allowing for the signals to be transmitted and received on the same side [20–25]. The most suitable incident angle corresponds to an angle slightly larger ($\approx 1^\circ$) than the first critically refracted angle [25].

In McGovern et al. [19], angle wedges were set to one degree above the respective first critical angle based on the amount of oxidative aging the specimen underwent. Because the ultrasonic velocities of asphalt concrete change with the level of oxidative aging [26], the first critical incident angle also changes correspondingly. Clearly, the aforementioned study [19] was performed with a prior knowledge of the level of oxidative-aging of the specimens. To apply this technique to the field for in-situ pavement testing, there is no prior knowledge of the oxidative-aging level of the asphalt concrete, rendering the appropriate incident angle also unknown. In this study, a systematic approach is proposed to address the issue of the unknown incident critical angle when there is access to only one side of the test specimen, *i.e.*, pavement. This method will allow the technique to be employed by practitioners in the field for pavement inspection, where the only preexisting knowledge of the pavement is its mixture-type. The use of a fixed angle removes the need to determine the critical angle, which reduces implementation time and makes it more practical for field use. Experimental validation is presented which support the validity of this approach.

2. Assessing the amount of oxidative aging in ac pavements via non-collinear wave-mixing of subsurface dilatational waves

To obtain the fundamental background of non-collinear wave-mixing, the reader is referred to references [13–18], and to references [19,27–32], where some applications can be found. When two monochromatic waves $\boldsymbol{k_1}$ and $\boldsymbol{k_2}$ with frequencies f_1 and f_2, respectively, are propagated in a medium with nonlinear elastic constants, such that they intersect at an angle φ, they can generate a scattered wave $\boldsymbol{k_3}$, with a sum or difference frequency ($f_3 = f_1 \pm f_2$). The scattered wave propagates at an angle γ with respect to $\boldsymbol{k_1}$. The type and polarization of the scattered wave depends on the type and polarization of the two primary waves. Jones and Kobett [14] found that for interaction to be possible, resonance and polarization conditions must be met. Consequently, out of fifty-four potential interaction cases, there are only nine interaction cases which satisfy both the resonance and polarization conditions.

In this study, two dilatational waves, $\boldsymbol{k_1}$ and $\boldsymbol{k_2}$, with frequencies f_1 and f_2, respectively, are transmitted such that they cross paths at an angle φ. In a nonlinear medium (*i.e.*, the higher order terms in the wave equation are not neglected), the two dilatational waves can interact to produce a third wave $\boldsymbol{k_3}$, with the frequency $f_3 = f_1 - f_2$. The third, scattered wave is a shear wave, polarized in the $\boldsymbol{k_1}$-$\boldsymbol{k_2}$ plane, and travels in the direction γ with respect to the direction of $\boldsymbol{k_1}$. For the case where two dilatational waves interact to produce a shear wave, the resonance and polarization conditions are met when the following two equations are satisfied,

$$\cos[\varphi] = \left(\frac{c_L}{c_S}\right)^2 \left[1 - \frac{1}{2}\frac{f_1}{f_2}\left(1 - \frac{c_S^2}{c_L^2}\right)\left(\frac{f_2^2}{f_1^2} + 1\right)\right] \tag{1}$$

$$\tan[\gamma] = \frac{-f_2 \sin[\varphi]}{f_1 - f_2 \cos[\varphi]} \tag{2}$$

where c_L and c_S are the dilatational and shear wave ultrasonic velocities of the medium, respectively. It is noted that the parameters of the two equations are interrelated, where when one is chosen (*e.g.*, φ), the other two are fixed (*e.g.*, f_2/f_1 and γ).

It has been shown that dilatational waves used for the interaction can be generated such that they propagate parallel to the surface by mounting the transducers on angle wedges set close to the first critically refracted angle [19]. A strong subsurface dilatational wave is generated by setting the incident angle 1° above the first critical angle [25]. Dilatational waves that propagate nearly parallel and near to the surface are also termed subsurface dilatational waves.

$$[\theta_{Inc.}]_{Critical} = \left[\sin^{-1}\left(\frac{c_{wedge}\sin(\theta_R)}{c_L}\right)\right]_{\theta_R = 90^\circ} \tag{3}$$

Two subsurface waves can be transmitted such that they interact and generate a third scattered shear wave, which propagates in the same plane as the two subsurface waves, *i.e.*, close to the surface. Implementing the non-collinear wave mixing technique in

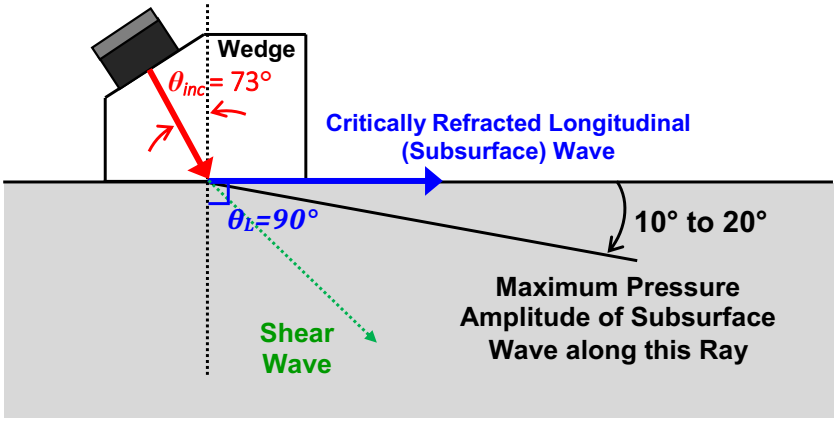

Fig. 1. Set-up employing use longitudinal transducers mounted on variable angle wedge coupled to the same side of the test specimen. Both wedges are set to the same angle, θ_{inc} = 73°.

this way allows for the nonlinear scattered wave to be received by a transducer mounted on the same side of the medium as the sending transducers. Thus, this technique is especially advantageous when there is only access to one side of the medium being assessed, such as the top surface of an AC pavement.

In the laboratory, the ultrasonic longitudinal and shear velocities and corresponding attenuations were characterized using a through-transmission technique with the sending and receiving transducers incidentally mounted on opposite and parallel sides of the test specimen [26]. The appropriate incident angle is typically found using Snell's Law (Eq. (3)) if the longitudinal acoustic velocities of the material being evaluated and of the wedge material are known. In the case of aged AC, the ultrasonic velocities and attenuations change as the amount of oxidative aging increases; therefore, the appropriate incident angle (*i.e.*, critical angle + 1°) varies and it depends upon the aging level of the test specimen.

Upon implementing the non-collinear wave mixing, it must be verified that the observed nonlinear response was a result from interaction between the bulk waves in the medium and not from nonlinearities in the testing apparatus. This verification can be accomplished by assuring that the criteria developed by Johnson and Shankland [27,28] are satisfied. These selection criteria include: (1) *amplitude criterion* – the amplitude of the nonlinear scattered wave must be proportional to the product of the two primary waves, (2) *frequency criterion* – the nonlinear scattered wave must have a frequency that matches that predicted by theory, and (3) *directionality criterion* – the nonlinear scattered wave must propagate in a direction that matches that predicted by theory. In addition to the selection criteria just listed, a *time-of-flight criterion* should also be used to assure that the wave arrives when expected, based on a straight ray path assumption. One of the advantages of using non-collinear wave mixing is to have frequency, directionality, and time-of-arrival separation of the resultant scattered wave from the two primary waves.

Two parameters of importance in assessing the amount of oxidative aging via the non-collinear wave mixing technique, are the frequency ratio, f_2/f_1, at which the nonlinear scattered wave is generated and the normalized nonlinear wave generation parameter, β/β_0. These two parameters are independent from each other. The frequency ratio is dependent on the material's ultrasonic velocities and interaction angle. The nonlinear wave generation parameter, β, represents conversion efficiency at which energy is converted from the two primary waves to the scattered nonlinear wave via the interaction and is found as,

$$\frac{\beta_{age}}{\beta_0} = \frac{A_{age}^{*(k_3)}}{A_0^{*(k_3)}} \tag{4}$$

where,

$$A_{age}^{*(k_3)} = \frac{A_{age}^{(k_3)}}{\exp[-(\alpha^{(k_1)} + \alpha^{(k_2)})D]\exp[-\alpha^{(k_3)}D_{k_3}]} \tag{5}$$

For simplification, in the above equation, the propagation distance of the two primary waves is assumed to be the same $D = D_{k_1} = D_{k_2}$. The attenuation coefficient is denoted by α, where the wavenumber is denoted by the superscript. The subscripts denote the amount of oxidative aging of the particular specimen (*i.e.*, the amount of hours aged). The attenuations are estimated using a through-transmission technique. Both β/β_0 and f_2/f_1 change as the level of oxidative aging changes, and therefore provide an indication of the amount of oxidative aging.

In a previous study [13], β/β_0 and f_2/f_1 were found for a set of six slab specimens extracted from gyratory compacted AC specimens with laboratory induced oxidative aging levels of 0, 12, 24, 28, 32, and 36 h, respectively. The slab samples (rectangular prisms of dimensions 150 × 175 × 50 mm) were all prepared with the same mixture, which had a target asphalt binder content of 5.9% by weight of the total mixture and 9.5-mm nominal maximum aggregate size. A β/β_0 versus f_2/f_1 plot was constructed to create a reference curve for that particular mixture.

For the current study, in addition to the six samples used to create the reference curve, three additional samples were prepared for a total of nine samples. The three new specimens were of the same mixture-type and geometry, and aged for 18, 26, and 30 h, respectively. The amount of oxidative aging of the samples were then assessed by determining where the (β/β_0, f_2/f_1) points lay on the reference curve to validate the method. It was assumed that there was no knowledge of the specimens' ultrasonic velocities and attenuations prior to taking the measurements.

3. Fixed incident angle technique

The main disadvantage to the non-collinear wave mixing approach to estimate levels of oxidative aging is the need for *a priori* knowledge of velocities and attenuations, which also depend upon the levels of aging. To address this difficulty, a new method, termed the "fixed angle technique" is introduced, where the wedges are set to a predetermined fixed incident angle based on the AC mixture type. In lieu of a fixed angle, the incident angle could be found experimentally via an iterative process; however, iteratively finding the suitable angle is time-consuming and tedious, as opposed to a fixed angle approach, which would be relatively easier to use in the field. The considerations in choosing this appropriate fixed angle is discussed in detail in the following sub-

sections. Once a suitable angle is found for a particular AC mixture type, it need not be found again. Linear parameters (*i.e.*, velocities and corresponding attenuations) are also necessary to be estimated to use the fixed angle approach. Once the linear parameters are estimated, then the subsurface non-collinear wave mixing technique can be employed as usual using the predetermined fixed angle.

3.1. Subsurface wave beam profile as a function of the incident angle

Following Chaki et al. [25], a dilatational subsurface wave is best generated by using a transducer mounted on an angle wedge with an incident angle of 1° larger than the first critical refracted angle. Theoretical and experimental studies have discussed the dependence of the beam profile upon deviations of the incident angle from the critical angle. References [20,22–25] provide detailed descriptions on the beam pattern as a function of the incident angle. This change in beam profile are now explained with regards to the aged AC sample set by way of two examples.

Consider the case where a plastic wedge with an incident angle of $\theta_{cr,virgin}$ is used, where $\theta_{cr,virgin}$ corresponds to the first critical angle for the virgin (*i.e.*, unaged) asphalt concrete sample. Let this same angle be used over the entire aged sample set. Recall that the velocities increase with increased aging from 0 to 24 h, after which the velocities decrease with increased aging [26]. This corresponds to a similar trend in the first critical angles, where the first critical angle decreases from 0 to 24 h, after which it increases with increased aging. Therefore, if an incident angle of $\theta_{cr,virgin}$ is used over the entire sample set, the following observations can be made. For the samples aged 12 and 24 h, the maximum displacement ray of subsurface wave will move closer to the surface, since their first critical angles are lower than that of the virgin sample. However, there is a counteracting effect: the main lobe of the ultrasonic beam becomes smaller in amplitude, narrower, and the side lobes become more dominant. For the specimens aged beyond 24 h (*e.g.*, 28, 32, and 36 h), the first critical angles are higher than the virgin sample. This means that for an incident angle of $\theta_{cr,virgin}$, the main lobe will increasingly move farther from the surface with increased aging. However, the main lobe also becomes wider, which combined with the already high beam spread means that a portion of the wave may still propagate parallel to the surface, in effect being a highly attenuated subsurface wave.

Now consider the case where the critical angle corresponding to the 36 h aged specimen, $\theta_{cr,36}$, is used across the entire asphalt concrete sample set. For the specimens aged 32 h and 36 h, a subsurface wave propagating nearly parallel to the surface will be generated, since the two have very similar dilatational velocities (<100 m/s difference for the 100–250 kHz range). The rest of the specimens (aged 0–28 h) have critical angles much lower than $\theta_{cr,36}$, with the farthest deviation being for the 24 h aged specimen, where $\theta_{cr,36} - \theta_{cr,24} \approx 29°$. As previously mentioned, the farther the incident angle is moved above the first critical angle, the more the side lobes begin to dominate. This means that any subsurface waves received at the surface of the specimens aged 0–28 h are probably due to the side lobes.

3.1.1. Incident angle

The variable angle wedges should be set to an incident angle such that non-collinear wave mixing of subsurface dilatational waves can take place, produce a nonlinear scattered shear wave, and that scattered wave can then be detected at the surface by a receiving transducer for the entire sample set of aged specimens (0–36 h aged). In a previous study [19], the first critical refracted angle was calculated for each aged specimen based on the corresponding empirically-measured velocities (see Table 1). Thus, there are six distinct critical angles corresponding to each of the six aged specimens, respectively.

To determine a suitable incident angle to use across the entire set of aged specimens, non-collinear wave mixing measurements should be performed for various incident angles. For each measurement, it should be determined if a nonlinear interaction took place by using the selection criteria developed by Johnson and Shankland [27,28]. These measurements should be taken with the goal of determining which angles could be used if there is no prior knowledge of the levels of aging of asphalt concrete samples. Since the material properties over the sample set of aged specimens (from 0 to 36 h) vary so significantly, one incident angle alone may not be sufficient to take usable measurements across the entire sample set; rather, measurements would need to be taken using more than one incident angle. Therefore, a goal in the selection of the incident angle should be to minimize the number of incident angles necessary to characterize the amount of oxidative aging in asphalt concrete aged in the range from 0 to 36 h for a particular mixture. This can be a time-consuming and tedious process; however, once performed, this angle will be a known suitable angle for that particular mixture type over a particular aged range. This angle will be referred to as θ_{inc} from this point forward.

3.2. Velocities and attenuations

In previous studies [19], experimentally measured attenuation [26] (as a function of aging and frequency) were used to normalize the scattered nonlinear wave amplitude in order to estimate the inherent nonlinearities. In this study, only one incident angle θ_{inc} is being used in the generation of the subsurface waves across the entire aged sample set. From the discussion in a previous section regarding the longitudinal subsurface beam profile as the incident angle is increased beyond the critical refracted angle, it is apparent that normalizing the amplitudes by the actual attenuations is an ambiguous task, unless there is *a priori* knowledge about the wave path (deviation from traveling parallel to the surface), wave field (the beam pattern changes with respect to aging), and amount of oxidative aging in the specimen. Therefore, to assess the amount of oxidative aging in asphalt concrete using the non-collinear wave mixing method, the "*perceived*" attenuation (*i.e.*, energy loss at the surface) should be estimated instead. This process of estimating the energy loss will now be described.

Consider a through-transmission set-up, where a sinusoidal toneburst (swept from 120 kHz to 200 kHz) is transmitted through the asphalt concrete specimen via a dilatational transducer mounted on an angle wedge. The signal propagates through the asphalt concrete, and it is received by another dilatational transducer mounted on the same side of the specimen. Both the sending and receiving dilatational transducers are mounted on variable angle wedges set to the predetermined incident angle θ_{inc} and

Table 1
Theoretically predicted critical angle + 1° based on Snell's law, and the experimentally determined critical angle + 1°.

Levels of oven-aging (h)	Theoretically Predicted Critical Angle + 1°* (°)
0	51
12	47
24	44
28	57
32	79**
36	73

* Based on literature [25], the angle at which the subsurface wave is able to be best detected, *i.e.*, maximum displacement at the surface, corresponds to around 1° above the first critical angle.

** Due to constraints with the angle wedges, the incident angle could not be greater than 75°.

spaced a prescribed distance apart that corresponds to the distance from the center of the wedge to the center of the region of interaction in the non-collinear wave mixing set-up, see Figs. 1 and 2.

As the wave propagates through the material, it suffers attenuation due to beam spread and inherent material attenuation (absorption and scattering). Since the case is being considered where there is only one incident angle across the entire sample set of aged specimens, the beam profile changes with respect to the amount of aging in the specimen. Accordingly, since the receiving transducer is placed on the same side of the specimen as the sending transducer, the perceived attenuation changes with aging as well, since the beam profile also changes. This energy loss at the surface is a function of the materials aging, the distance the wave travels, the incident angle, and the frequency.

$$\mu = \mu(f, d, \theta_{Inc.}, age) \tag{6}$$

Thus, the received amplitude for a subsurface dilatational wave sent by transducer mounted on an angle wedge with an incident angle of θ_{inc}, received by a transducer mounted on an angle wedge with the same angle, propagated at a distance D with frequency f can be expressed as,

$$[A_{age}(f, D, \theta_{Inc.})]_{Thr-Trans} = A_{Sent} e^{-\mu_L(f,D,\theta_{Inc.},age)\cdot D} \tag{7}$$

where the subscript L denotes a longitudinal wave. Normalizing above equation by the received amplitude through the virgin specimen,

$$\left[\frac{A_{age}(f, D, \theta_{Inc.})}{A_0(f, D, \theta_{Inc.})}\right]_{Thr-Trans} = \frac{e^{-\mu_L(f,D,\theta_{Inc.},age)\cdot D}}{e^{-\mu_L(f,D,\theta_{Inc.},0)\cdot D}} \tag{8}$$

Eq. (8) describes the normalized energy loss at the surface in a through-transmission set-up for dilatational waves.

The "*perceived*" energy loss of shear waves through the material must also be estimated. Shear subsurface waves should not be used to measure the shear wave attenuation due to inaccuracies arising from interaction with the free surface (*e.g.*, mode conversion into dilatational waves). Furthermore, conventional wedges (*e.g.*, plastic) cannot be used, as very low wedge ultrasonic velocities would be required to generate subsurface shear waves that would propagate parallel to the surface. The shear attenuation can be estimated via an empirical relation between the longitudinal velocity and shear attenuation coefficient,

$$\alpha_S(60\ \text{kHz} \leqslant f \leqslant 90\ \text{kHz}) \approx -0.031 c_L + 152.991 \tag{9}$$

This empirical relationship is only valid for the AC mixture-type of the sample set used in this study, for α_s in a frequency range of 60–90 kHz (which corresponds to the range of the nonlinear shear wave frequencies in this study), and for the longitudinal velocity above the frequency at which it becomes non-dispersive (*i.e.*, frequency independent). The longitudinal velocity was related to the shear attenuation instead of the longitudinal attenuation, because although α_L is proportional to α_s, the proportionality constant is not the same across the entire sample set of aged specimens. The longitudinal velocities can be estimated by measuring the time-of-flight of through-transmission subsurface wave. Since this method only uses one incident angle θ_{inc} across the entire sample set, there may be large errors in the longitudinal wave velocity estimate due to a change in the beam profile. The validity of this technique is based on the principle that the fastest arriving portion of the wave should be the longitudinal component of the wave that travels the most parallel to the surface.

3.3. Non-collinear wave mixing

Once the mixture-type of the pavement is identified, θ_{inc} is known for that mixture, and the non-collinear wave mixing technique can be employed as usual. It is crucial to verify that the received nonlinear wave satisfies the selection criteria. The primary wave frequency ratio (f_2/f_1) at which the nonlinear wave amplitude is the largest should not be dependent on the incident angle. Thus, f_2/f_1 can be found by determining the point at which the nonlinear wave amplitude reaches a maximum as f_2 is swept.

The amplitude of the scattered nonlinear wave is proportional to the product of the amplitudes of the two interacting primary waves [14–17]. For simplicity, it is assumed that both primary waves, *i.e.*, $\boldsymbol{k_1}$ and $\boldsymbol{k_2}$, travel the same distance D (measured from the center of the wedge to the center of interaction volume). Recalling that the energy loss at the surface is a function of the distance and frequency, the amplitude of the nonlinear scattered wave can be written as,

$$[A_{age}^{(k_3)}]_{\theta_{Inc.}} = \beta_{age} A_{sent}^{(k_1)} A_{sent}^{(k_2)} e^{(-\mu_L(f_1,D,\theta_{Inc.},age) - \mu_L(f_2,D,\theta_{Inc.},age))\cdot D} e^{-\mu_S(f_3,D_{k_3},\theta_{Inc.},age)\cdot D_{k_3}} \tag{10}$$

The subscripts L and S denote dilatational and shear waves, respectively. The expression above can be similarly written for the unaged sample. Normalizing by the amplitude of received nonlinear scattered wave with the corresponding scattered wave amplitude obtained in the unaged specimen yields,

$$\left[\frac{A_{age}^{(k_3)}}{A_0^{(k_3)}}\right]_{\theta_{Inc.}} = \frac{\beta_{age}}{\beta_0} \frac{e^{-\mu_L(f_1,D,\theta_{Inc.},age)\cdot D}}{e^{-\mu_L(f_1,D,\theta_{Inc.},0)\cdot D}} \frac{e^{-\mu_L(f_2,D,\theta_{Inc.},age)\cdot D}}{e^{-\mu_L(f_2,D,\theta_{Inc.},0)\cdot D}} \times \frac{e^{-\mu_S(f_3,D_{k_3},\theta_{Inc.},age)\cdot D_{k_3}}}{e^{-\mu_S(f_3,D_{k_3},\theta_{Inc.},0)\cdot D_{k_3}}} \tag{11}$$

Using the empirical relation from Eq. (9) as an approximation to estimate the shear wave attenuation gives:

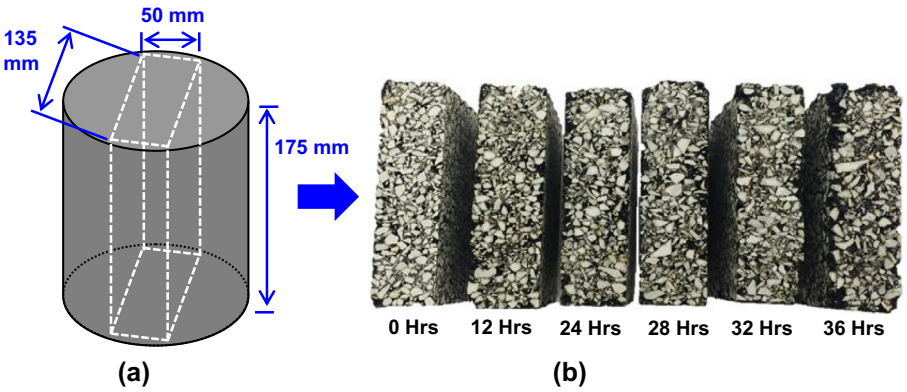

Fig. 2. Test specimens; (a) gyratory compacted samples and (b) test specimens with different levels of oven aging.

$$\frac{e^{-\mu_S(f_3,D_{k_3},\theta_{Inc.},age)\cdot D_{k_3}}}{e^{-\mu_S(f_3,D_{k_3},\theta_{Inc.},0)\cdot D_{k_3}}} \approx \frac{e^{-\alpha_S(c_L(age))\cdot D_{k_3}}}{e^{-\alpha_S(c_L(0))\cdot D_{k_3}}} \tag{12}$$

This approximation will be an underestimate, *i.e.*, a lower bound, of the perceived attenuation (*i.e.*, energy loss at surface), because the empirical relationship does not account for the beam pattern or the fact that the shear wave does not necessarily propagate parallel to the surface. Substituting the relationships from Eqs. (8) and (12) into Eq. (11) leads to:

$$\left[\frac{A_{age}^{(k_3)}}{A_0^{(k_3)}}\right]_{\theta_{Inc.}} \approx \frac{\beta_{age}}{\beta_0}\left[\frac{A_{age}(f_1,D,\theta_{Inc.})}{A_0(f_1,D,\theta_{Inc.})}\frac{A_{age}(f_2,D,\theta_{Inc.})}{A_0(f_2,D,\theta_{Inc.})}\right]_{Thr-Trans} \times \frac{e^{-\alpha_S(c_L(age))\cdot D_{k_3}}}{e^{-\alpha_S(c_L(0))\cdot D_{k_3}}} \tag{13}$$

Thus,

$$\frac{\beta_{age}}{\beta_0} \approx \left(\left[\frac{A_{age}^{(k_3)}}{A_0^{(k_3)}}\right]_{\theta_{Inc.}}\right)\left[\frac{A_0(f_1,D,\theta_{Inc.})}{A_{age}(f_1,D,\theta_{Inc.})}\frac{A_0(f_2,D,\theta_{Inc.})}{A_{age}(f_2,D,\theta_{Inc.})}\right]_{Thr-Trans}\left(\frac{e^{-\alpha_S(c_L(0))\cdot D_{k_3}}}{e^{-\alpha_S(c_L(age))\cdot D_{k_3}}}\right) \tag{14}$$

Due to the approximations, $\frac{\beta_{age}}{\beta_0}$ is only an estimate of the actual normalized nonlinear wave generation parameter. Note that f_1 and f_2 are known, as the f_2/f_1 peak is found during the use of the non-collinear wave-mixing process. Therefore, the primary wave attenuation estimates should be used at the appropriate frequencies.

Prior to taking field measurements, it is assumed that the parameters for unaged AC in the above equations are known, whether by laboratory measurements performed on specimens of the same mix-type, or measurements performed on test samples made of the protected bottom layer from extracted field cores. These values should be found using the same testing set-up as used in the field so as to be consistent with the equations above. Then, the measured point (f_2/f_1, β/β_0) can be plotted on the reference curve, where its relative location allows the estimation of the pavement top layer oxidative aging level.

3.4. Advantages and disadvantages of the fixed angle technique

The biggest advantage of the fixed angle technique is the ease at which it can be implemented, rendering it ideal for field use. However, there are drawbacks in terms of its accuracy. Although the f_2/f_1 ratio metric does not suffer using this method, the estimation of the β/β_0 parameter suffers due to relative larger errors in the attenuation estimates. Another drawback to fixed angle technique is that although the chosen incident angle may be ideal for a small range of aged specimens, it is not the best possible angle for generating subsurface longitudinal waves for the entire aged sample set. This may have the effect of making it more difficult to detect the nonlinear wave for specimens with critical angles far from the chosen incident angle. In addition, for other AC mixture-types, more than one incident angle may be necessary to achieve a wide range of aging-assessment. The fixed angle technique also tends to be sensitive to non-uniformities in the aging process. The most suitable incident angle is not necessarily being used; thus, multiple peaks in the frequency ratio versus amplitude curve may be detected which may complicate the analysis.

4. Experimental set-up

Six asphalt concrete specimens were prepared with the same mixture of 9.5-mm nominal maximum aggregate size and a target asphalt content of 5.9% by total weight of the mixture. The binder used was Superpave PG 64-22 and the aggregates were from four different stockpiles sampled in central Illinois: 65% of coarse aggregate (CM16), 23% of manufactured sand (FM20), 10.5% of natural sand (FM02), and 1.5% of mineral filler (MF).

Mixing was accomplished using a standard bucket mixing procedure at a temperature of 155 °C. The mixtures were then subjected to oxidative aging by placing them in an oven at 135 °C. Each mixture was aged a different amount of time: 0, 12, 24, 28, 32, and 36 h. The mixtures were hand-stirred every 12 h to ensure uniform exposure of the mixture to oxygen (*i.e.* uniform aging process). Six cylindrical specimens (180 mm height and 150 mm diameter) were created by compacting the aged mixtures with a servo-controlled gyratory compactor (IPC Servopac) at a temperature of 135 °C. As illustrated in Fig. 2, each cylinder was then cut to obtain a rectangular prism with dimensions 155 × 175 × 50 mm. Six asphalt specimens constructed with same mixture design and oxidative aging via the manner above were characterized using linear ultrasonics in a previous study [20], where the ultrasonic phase velocities and attenuations for longitudinal and shear waves from that study were determined as a function of frequency.

In a previous study [19] an "ideal" testing set-up was found. This testing set-up was based on the parameters for unaged specimens of this particular mixture type and held constant over all aged specimens. In addition, it was also ensured that, regardless of specimen aging level (between 0 and 36 h), the scattered ultrasonic wave beam was always received by the receiving transducer, *i.e.*, the scattered wave angle did not deviate excessively. Please see McGovern et al. [19] for a more detailed discussion on choosing a suitable testing set-up for a sample set with AC specimens of various oxidative aging.

Fig. 3 shows a schematic diagram of the data acquisition system used in this study. A pulser-receiver (Ritec – RPR 4000) was used to generate a 15-cycle sinusoidal toneburst at f_1 = 200 kHz, which was sent to a dilatational transducer (Panametrics V413, with a center frequency of 500 kHz) mounted on a variable angle wedge (Panametrics ABWX-2001, longitudinal velocity = 2720 m/s). A function generator (Krohn-Hite Model 5920) was used to generate an 8-cycle sinusoidal toneburst, which swept from f_2 = 100 kHz to 180 kHz in 1 kHz increments. A gated amplifier (Ritec GA-2500A) was used to amplify the signal and send it to another dilatational transducer (Panametrics V413, with a center frequency of 500 kHz), also mounted on a Plexiglas variable angle wedge (Panametrics ABWX-2001, longitudinal velocity = 2720 m/s). The variable angle wedges were set to an incident angle of 73°. The two wedges were oriented such that the primary waves ($\boldsymbol{k_1}$ and $\boldsymbol{k_2}$) traveled for a distance of 8.2 cm (from the center of the wedge to the center of the volume of interaction) and they interacted at an angle of φ = 47°. The receiving transducer (Panametrics V1011, center frequency of 100 kHz) placed on the same face and oriented at γ = −37° (with respect to $\boldsymbol{k_1}$) so that it intercepted the nonlinear scattered shear wave $\boldsymbol{k_3}$, which propagated a distance of 4 cm (from the center of the volume of interaction to the center of the transducer face). The received signal was amplified and filtered using a 2nd-order Butterworth filter (Krohn Hite Model 3945). An average of 300 signals was taken to mitigate effects from scatter.

The following steps were taken for the data collection: (1) the signal was obtained while both transducers were operated simultaneously, (2) the signal was obtained operating only one transducer, and (3) the signal was then obtained while operating the other transducer. The signals obtained from (2) and (3) were then subtracted from the signal obtained in (1) to obtain the nonlinear scattered wave.

Prior to implementing the fixed-angle technique, the f_2/f_1 versus β/β_0 reference curve was generated. Once this reference curve is generated, it need not be generated again as long as the testing set-up and mixture-type remain the same. The procedure is as follows: (1) identify the mixture type for the asphalt concrete to be assessed; (2) set the angle wedges to the predetermined angle θ_{inc} for this mixture type; (3) determine the energy loss at the surface using the technique described in Section 3 across a range of frequencies with the wedges set to θ_{inc}; (4) Obtain an estimate for the dilatational velocity using through-transmission of the wedges set to θ_{inc}, and use Eq. (9) to obtain an estimate of the shear attenuation; (5) perform the non-collinear wave mixing technique using the testing set-up described above with the wedges set to θ_{inc}; (6) determine the f_2/f_1 at which the maximum nonlinear wave amplitude occurs; (7) correct the nonlinear wave amplitude for the attenuation at the appropriate frequencies using Eq. (14) and the attenuation/energy loss estimates obtained in Steps 3 and 4 to obtain β/β_0. Note that the β_0 is known, as it is previously determined from a virgin specimen in the laboratory for this known mixture type using the same testing set-up; (8) plot the point (f_2/f_1, β/β_0) on the reference curve and see where the point lies to determine the aging level.

5. Experimental results

Prior to implementing the fixed-angle technique, laboratory measurements were performed on the sample set using the known attenuation and velocity values [26]. An f_2/f_1 versus β/β_0 reference curve was generated and is denoted by the solid black line in Fig. 4, where the error boxes indicate the maximum and minimum measurements. These results are discussed in more detail in McGovern et al. [19]. A "blind study" was then performed using the fixed angle technique on the laboratory aged specimens in the same manner as it would be performed in the field. In other words, it was assumed that there was no knowledge of the specimens' aging or linear ultrasonic parameters (velocity and attenuation) *a priori*.

A study was performed to determine which incident angle(s), if any, could be used to implement subsurface non-collinear wave mixing across the entire age range (0–36 h of oven-aging) of the samples in the set. For each aged specimen,

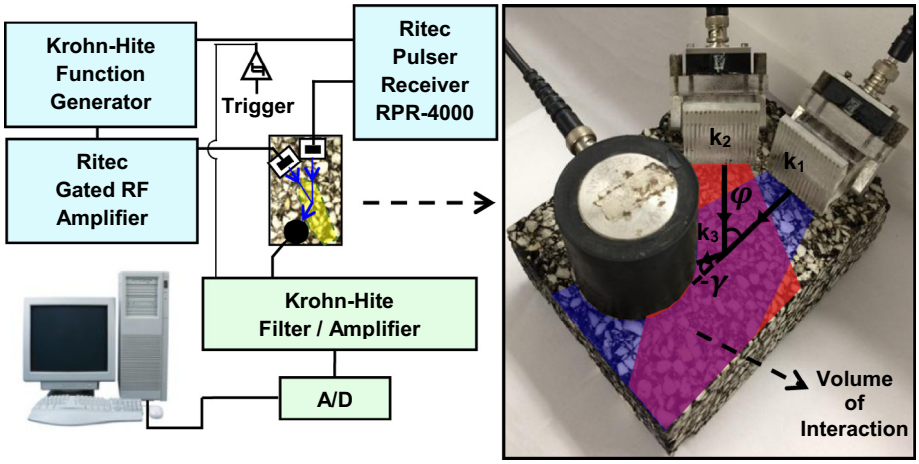

Fig. 3. Schematic diagram of the ultrasonic non-collinear wave mixing data collection system illustrating the angle of interaction of the two longitudinal waves and the location of the shear transducer to receive the generated scattered shear wave. The blue and red regions denote the regions of the primary waves $\boldsymbol{k_1}$ and $\boldsymbol{k_2}$, respectively, due to beam spread. The region where they overlap is the volume of interaction. Note that the beam spread from $\boldsymbol{k_2}$ is slightly higher than $\boldsymbol{k_1}$ due to the difference in frequencies. (For interpretation of the references to color in this figure legend, the reader is referred to the web version of this article.)

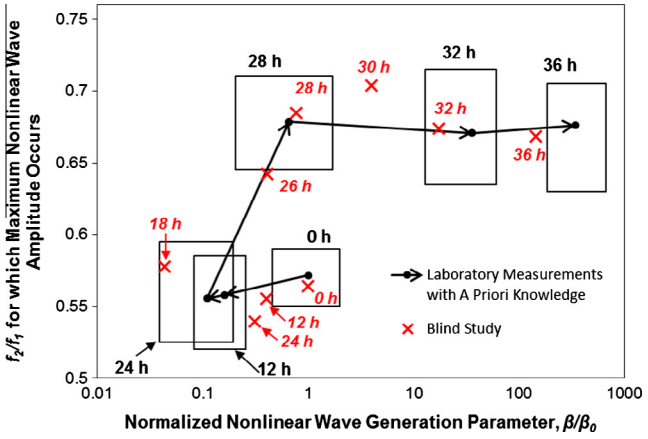

Fig. 4. The frequency ratio f_2/f_1 at which maximum amplitude of the scattered nonlinear wave occurs vs. the nonlinear wave generation parameter β, normalized by the value corresponding to the un-aged mixture β_0 for asphalt concrete specimens subjected to oven-aging. The figure represents the evolution of the nonlinearities, *i.e.*, damage, associated with oven-aging. The trajectory of damage accumulation for an increasing number of hours of oven-aging is mixture dependent. The solid dots represent an average of 10 independent measurements. The intervals of confidence represent the maximum and minimum of these 10 independent measurements. These values were obtained using the subsurface longitudinal waves at the respective critical angles for each specimen [20]. Normalization by attenuation was done using Eq. (14), assuming a straight ray path propagation, and assuming that the waves propagated nearly parallel to the surface of the specimen. The red *x*'s represent the average of the 10 independent measurements taken from the top surface without any prior knowledge of the specimen aging (only the type of mixture was known). (For interpretation of the references to color in this figure legend, the reader is referred to the web version of this article.)

non-collinear wave mixing measurements were taken using all 6 incident angles listed in Table 1. Five independent measurements were taken for each test. Amplitudes of the nonlinear scattered wave signal $\boldsymbol{k_3}$ were recorded by passing the difference signal (*i.e.*, scattered wave) through a band-pass filter centered about the range of expected f_3's (for 0–36 h) as f_2 was swept and f_1 was held constant. The amplitude-versus-frequency ratio plots were then "stacked" to create a surface plot. Fig. 5 shows surface plots created by using (a) incident angles set to each respective samples' critical angle for a baseline comparison, and incident angles set to the critical angle corresponding to (b) 0 h aging level (51°), (c) 24 h aging level (44°), and (d) 36 h aging level (73°). The grayscale denotes the normalized amplitude, where each specimens' amplitude was normalized by its own maximum (in the range over which f_2 swept). Thus, the surfaces reflect the shape of the $\boldsymbol{k_3}$ amplitude and not the absolute magnitude. If this normalization were instead done using the maximum value of all of the specimens, the normalized amplitude of the difference signal for the higher aging level specimens would be relatively small (due to higher attenuations), which would impair the visualization. The expected frequency ratios are superimposed on the figures and denoted by a solid black line. These expected frequency ratios correspond to the observed frequency ratios in the baseline figure, Fig. 5.a. For the baseline measurements (Fig. 5.a), it was observed that for the higher aged specimens, there is more of a "spread" in the frequencies observed. This may be due to nonuniform aging in the mixture of the test sample, which would have the effect of causing interactions at various frequencies for the same interaction angle.

The volume of interaction is a function of the specimen dimensions and transducer beam divergence (see Fig. 4 for an illustration of the interaction region). Considering the beam divergence, as the angle between the transducer centerline and the point where the signal is half its strength, a characteristic length of the volume of interaction can be estimated at the point where the two primary beams intersect. The most limiting case corresponds to the specimen aged 24 h, which corresponds to the longest wavelengths. Comparing this characteristic length with the number of possible signal wavelengths within the region of interaction, the characteristic length of the volume of interaction is always greater than 3.5 times the largest signal wavelength, *i.e.*, $\boldsymbol{k_2}$, for the entire test sample set. For all non-collinear wave mixing measurements, Johnson and Shankland's selection criteria [27,28] was used to verify that the nonlinear waves arose from the primary wave interaction. It was verified that all of the difference signals met the frequency, amplitude, directionality, and time-of-arrival criteria.

The measurements taken using the incident angles corresponding to 0, 24, and 36 h are shown in Fig. 4.b, 4.c, and 4.d, respectively, as these samples bound the entire sample set. The samples aged 0 and 36 h characterize the extremes of the sample set in terms of aging, and the samples aged 24 and 36 h characterize the bounds in terms of their respective critical angles. For the incident angle corresponding both the 0 and 24 h aged specimen (Fig. 4.b and 4.c, respectively), it was observed that these incident angles work well for specimens aged 0–24; however, they do not work well for specimens aged beyond 24 h.

For the mixture type and angle wedges used in this study, it was found that an incident angle of 73° was the best suited angle to show the nonlinearities across the entire sample set (Fig. 5.d). It is hypothesised that the reason the 73° angle works across the entire sample set is due to interaction of the side-lobes present in the subsurface beam. As the incident angle is moved beyond the first critical refracted angle, the side lobes begin to dominate [24,25]. The presence of side lobes, along with the large beam spread in the sample, may cause the scattered wave to be generated and received at the surface for incident angles much larger than the critical refracted angle. The nonlinearities in the sample aged for 24 h were most difficult to observe at this angle due to a relatively low amplitude. However, this was not unexpected, as this sample's critical angle has the largest deviation from the incident angle (*i.e.*, 73° − 44° = 29°), as shown in Table 1. The nonlinear response in the sample aged 28 h was slightly more difficult to investigate, as multiple pronounced peaks in the frequency spectra of the resultant scattered wave were observed. This is most likely due to non-uniformities in the aging of the mixture in that particular test sample.

For the measurements taken using an incident angle of 73°, the two nonlinear parameters, f_2/f_1 and β/β_0, were found for the entire sample set. The f_2/f_1 was found by determining the point at which the nonlinear wave amplitude reached a maximum as f_2 was swept and f_1 was held constant. The β/β_0 was found using the amplitude ratios as defined in Section 3. These amplitude ratios define the energy loss observed at the surface. Table 2 shows the experimentally recorded amplitude

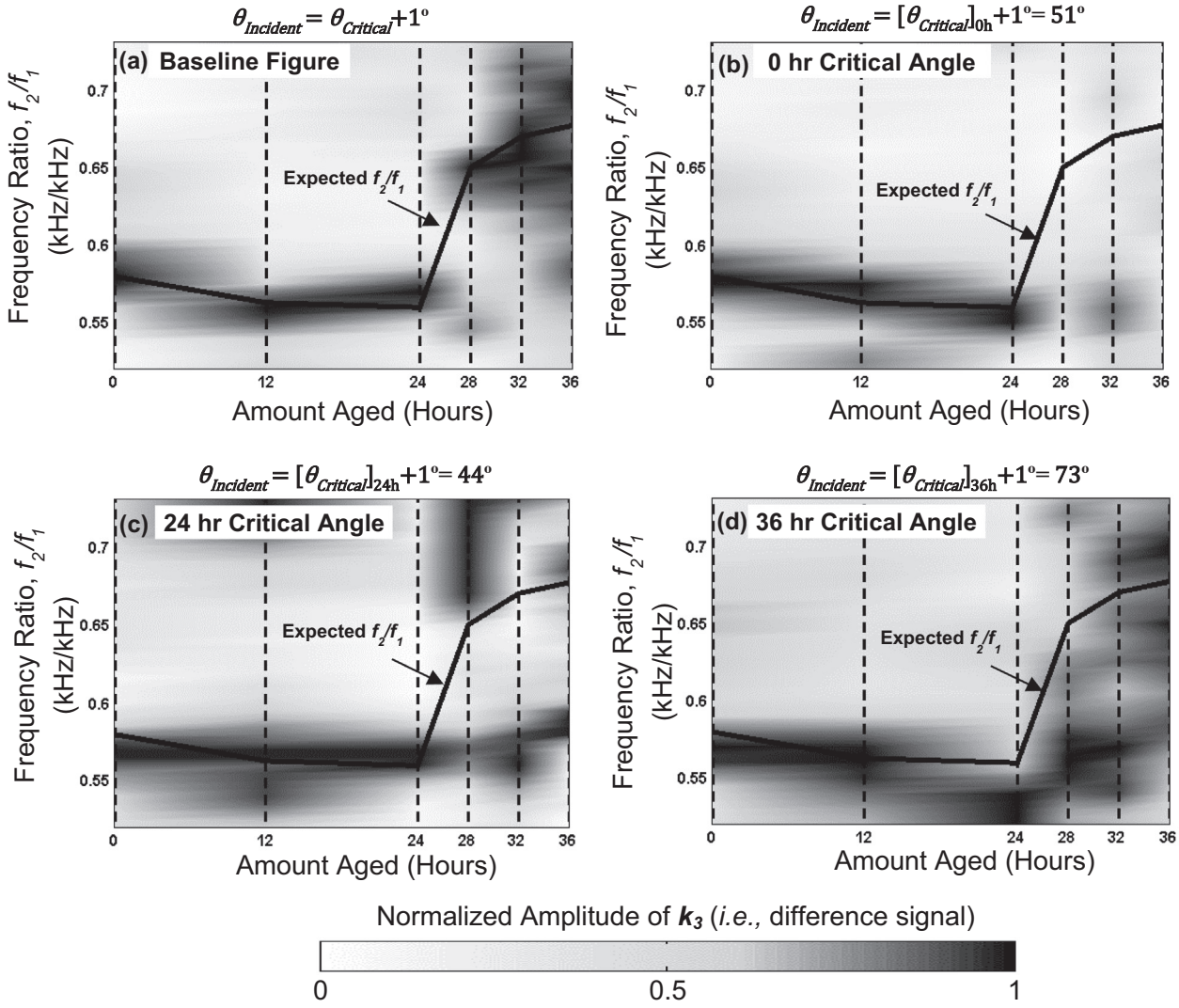

Fig. 5. Frequency ratio vs. aging level (hours) showing the expected f_2/f_1 ratio based on experimentally obtained critical angles. The figures also show the color coded amplitude (A) of the scattered wave in the axis perpendicular to the plane. For each aging level sample, these amplitudes are normalized using the maximum value for that sample, see normalized bar code of the difference signal. This was done to enhance visualization of the results, but prevents comparison of the difference signal amplitudes among the test specimens. The color code representation in the graph is a linear interpolation of the values obtained for the discrete levels of aging. Please note that at each aging level, along the dashed vertical lines, the color code is normalized from 0 to 1. Figure (a) was obtained using the correct critical angle for each aging level for each specimen. Figures (b), (c), and (d) represent the amplitude of the difference signal when the critical angle for the virgin, 24, and 36 h of aging, respectively, are used for all of the specimens.

ratios. The dilatational velocities were estimated using a through-transmission set-up, and the values are shown in Table 3. Note the relatively high errors. Because only one incident angle was used across the entire set (*i.e.*, an angle equal to 73°, which corresponds to the critical angle for the 36 h aged sample), the subsurface wave did not necessarily travel parallel to the surface for the samples that were aged less than 36 h; consequently, the measured velocity was an underestimate of the actual velocity. Also, for the specimens with the lowest amounts of aging (0–24 h), the incident angle is so far beyond the first critical angle that the side lobes dominate and effectively become the new main lobe. This drastic change in

Table 2
Dilatational energy loss and shear attenuation for different aging levels at the corresponding f_3 frequency.

Levels of oven-aging (h)	Measured Normalized Dilatational Energy Loss at Surface using Through-Transmission Angle-Wedge Set-up $\left[\frac{A_{age}(f_1,D)}{A_0(f_1,D)}\frac{A_{age}(f_2,D)}{A_0(f_2,D)}\right]_{Incident} = \frac{e^{-\alpha'_L(f_1,D,age)\cdot D}}{e^{-\alpha'_L(f_1,D,0)\cdot D}}\frac{e^{-\alpha'_L(f_2,D,age)\cdot D}}{e^{-\alpha'_L(f_2,D,0)\cdot D}}$	Shear Attenuation Coefficient Based on Empirical Relationship with Subsurface Dilatational Velocity, α_S (Np/m)
0	1.00	51.6
12	2.05	44.8
24	2.07	42.5
28	0.91	44.8
32	0.14	73.9
36	0.02	69.8

Table 3
Dilatational velocities using a normal incidence through-transmission technique.

Levels of oven-aging (h)	Experimentally Measured using Normal Incidence Through-Transmission Set-up [19] (m/s)	Experimentally Measured from Longitudinal Subsurface Waves in a Through-Transmission Set-up (m/s)	Percent Error (%)
0	3554	3252	8.51
12	3792	3472	8.43
24	4007	3546	11.50
28	3284	3472	5.73
32	2780	2534	8.85
36	2861	2667	6.78

the beam pattern introduced errors in the velocity measurements. The shear wave attenuations were estimated using the empirical relationship with the experimentally estimated subsurface dilatational velocities. The energy loss at the surface was measured directly using the technique described in Section 3.

Fig. 4 contains the results from the blind study, where these measurements are denoted by the red "x's". As expected, the specimens with the lowest amounts of aging (0–24 h) deviate the most from the laboratory determined reference curve due to the large deviations in the first critical angle with respect to the incident angle.

For the purposes of pavement management, it would be advantageous to have a non-destructive technique to determine when an asphalt pavement is no longer able to self-heal, *i.e.*, to determine when a permanent damage state has been reached in the pavement surface. The accuracy of the proposed method appears to be sufficient to make this determination if applied periodically throughout the life of the pavement surface. For instance, a study by Braham et al. [33] showed that the 24-h oven aging level represented approximately 7 years of field aging. In some of the sections investigated, the field aging experienced at 7 years was sufficient for the development of temperature-induced thermal cracking. This conclusion was based upon fracture energy testing of asphalt-aggregate mixtures, where field-aged core samples, field cracking versus time data, and original materials stored at the time of pavement construction were available. Original materials were oven-aged to develop a fracture energy versus time relationship, which was then compared to fracture energy levels of materials sampled from 7-year aged field sections. Based on observed field cracking, it appears that 24 h of oven-aging represents an aging level where permanent damage may be retained in the asphalt mixture. This seems to correspond to the shift observed in Fig. 5 between the 24 and 28 h aging when plotted in the f_2/f_1 vs. β/β_0 space. Measurements taken on samples aged at 0, 12 and up to 24 h fell in the lower plateau range, with 24-h of oven-aging representing a breakpoint between the lower and upper plateau regions on Fig. 5.

A possible application of this technique in pavement engineering might involve the use of nonlinear ultrasonics to assess and treat asphalt pavement surfaces (such as using penetrating rejuvenators), to retain material behavior safely in the right-hand side of the lower plateau (healing region), *i.e.*, in the 0–12 equivalent oven-aging regime. This would prevent allowing the pavement surface to age to a condition where permanent damage and the vulnerability towards large, discrete crack formation (such as thermal and block cracks) to occur. It is envisioned that a number of the experimental and analysis steps presented herein could be fully automated or further simplified with additional testing, validation, and development of practitioner-friendly equipment and software. A relatively low-cost, portable test system appears to be feasible, which would provide practitioners with a new and powerful tool for in-situ evaluation of asphalt pavement surfaces and strategic timing of preventive maintenance treatments.

6. Conclusions

A previous study [19] demonstrated the feasibility of using the non-collinear wave mixing of subsurface dilatational waves as a way to assess the amount of oxidative aging of asphalt concrete. Subsurface dilatational waves can be generated by implementing transducers mounted on angle wedges, and the resulting nonlinear scattered wave can be received by a transducer placed on the same side. Thus, this technique is truly non-destructive, in that it only requires access to one side (*i.e.*, the top) of the pavement. The angle wedges must be set to an angle close to the first critical angle for dilatational waves to be generated, which requires knowledge of the dilatational velocity of the AC pavement. In this study, a new method presented, which allows for the non-collinear wave mixing technique to be employed when the only prior knowledge of the AC pavement is the mixture type. The technique proposed in this study involves the use of one fixed incident angle. As usual, the nonlinear scattered waves which arose from the wave-mixing were checked to ensure that they arose from the wave-mixing and not the testing apparatus by using Johnson and Shankland's selection criteria [27,28]. As in reference [19], the presented technique also uses two metrics, f_2/f_1 and β/β_0 as a means to assess the oxidative aging by determining their location on a previously generated β/β_0 versus f_2/f_1 reference curve for that mixture type. The fixed angle technique, although less accurate than the conventional non-collinear wave mixing technique, is faster and more practical for field use.

Acknowledgements

The authors are grateful for the partial support of the US Airforce Civil Engineering Center (AFCEC) including the technical support of our technical contact Dr. George Vansteenburg. The authors are also very grateful for the technical support of Dr. Jeb S. Tingle (ERDC-RDE-GSL-MS). Any opinions, findings and conclusions or recommendations expressed in this publication are those of the authors and do not necessarily reflect the views of the sponsoring agency.

References

[1] D.Y. Lee, Development of a durability test for asphalts, Iowa Highway Research Board Project HR-124, Final Report ISU-ERI-72125, Engineering Research Institute, Iowa State University, 1972.
[2] D.Y. Lee, Weathering of asphalts as characterized by infrared multiple internal reflection spectra, Appl. Spectrosc. 27 (6) (1973) 435–440.
[3] E.R. Brown, P.S. Kandhal, F.L. Roberts, Y.R. Kim, D. Lee, T.W. Kennedy, Hot Mix Asphalt Materials, Mixture, Design, and Construction, third ed., NAPA Research and Education Foundation and NCAT, Maryland, 2009.
[4] R.Y. Kim (Ed.), Modeling of Asphalt Concrete, American Society of Civil Engineers Press and McGraw Hill, Chicago, 2009.
[5] R.A. Guyer, P.A. Johnson, Nonlinear Mesoscopic Elasticity: The Complex Behavior of Granular Media Including Rocks and Soil, Wiley-VCH, Weinheim, 2009.
[6] R.A. Guyer, P.A. Johnson, Nonlinear mesoscopic elasticity: evidence for a new class of materials, Am. Inst. Phys., Phys. Today 52 (4) (1999) 30–36, http://dx.doi.org/10.1063/1.882648.
[7] S. Kose, M. Guler, H.U. Bahia, E. Masad, Distribution of strains within hot-mix asphalt binders— applying imaging and finite element techniques, Transportation Research Board (2000) 21–27. paper no. 00-1391.
[8] E. Masad, N. Somadevan, H.U. Bahia, S. Kose, Modeling and experimental measurements of strain distribution in asphalt mixes, J. Transp. Eng. 127 (6) (2001) 477–485.
[9] E. Masad, C.-W. Huang, G. Airey, A. Muliana, Nonlinear viscoelastic analysis of unaged and aged asphalt binders, Constr. Build. Mater. 22 (2008) 2170–2179.
[10] Rodrigo Delgadillo, Nonlinearity of Asphalt Binders and their relationship with Asphalt Mixture Permanent Deformation Ph.D. Thesis, University of Wisconsin, Madison, 2008.
[11] F.D. Murnaghan, Finite Deformation of an Elastic Solid, John Wiley & Sons Inc, New York, 1951.
[12] L.D. Landau, E.M. Lifshitz, Theory of Elasticity, second ed., Pergamon Press, New York, 1970.
[13] Z.A. Gol'dberg, Interaction of plane longitudinal and transverse elastic waves, Sov. Phys. Acoust. 6 (3) (1960) 306–310.
[14] G.L. Jones, D.R. Kobett, Interaction of elastic waves in an isotropic solid, J. Acoust. Soc. Am. 35 (1) (1963) 5–10.
[15] L.H. Taylor, F.R. Rollins, Ultrasonic study of three-phonon interactions. I. Theory, Phys. Rev. 136 (3A) (1964) A591–A596.
[16] F.R. Rollins, L.H. Taylor, P.H. Todd, Ultrasonic study of three-phonon interactions. II. Experimental results, Phys. Rev. 136 (3A) (1964) A597–A601.
[17] F.R. Rollins, Phonon interactions and ultrasonic frequencies, Proc. IEEE 53 (10) (1965) 1534–1539.
[18] L.K. Zarembo, V.A. Krasil'nikov, Nonlinear phenomena in the propagation of elastic waves in solids, Sov. Phys. 13 (6) (1970) 778–797.
[19] M.E. McGovern, W.G. Buttlar, H. Reis, Estimation of oxidative aging in asphalt concrete pavements using non-collinear wave mixing of critically refracted longitudinal waves, INSIGHT-Non-Destructive Test. Cond. Monitor. J. 56 (7) (2014) 367–374.
[20] D.E. Bray, R.K. Stanley, Nondestructive Evaluation, revised edition., CRC Press, Inc., Boca Raton, 1997.
[21] J.L. Rose, Ultrasonic Waves in Solid Media, Cambridge University Press, New York, 1999.
[22] L. Basatskaya, I. Ermolov, Theoretical study of ultrasonic longitudinal subsurface waves in solid media, Sov. J. Nondestr. Test. 16 (1981) 524–530.
[23] A. Pilarski, J. Rose, Utility of subsurface longitudinal waves in composite material characterization, Ultrasonics 27 (1989) 226–233.
[24] K. Langenberg, P. Fellinger, R. Marklein, On the nature of the so-called subsurface longitudinal wave and/or the subsurface longitudinal "creeping" wave, Res. Nondestr. Eval. 2 (1990) 59–81.
[25] S. Chaki, W. Ke, H. Demouveau, Numerical and experimental analysis of the critically refracted longitudinal beam, Ultrasonics 53 (2013) 65–69.
[26] M.E. McGovern, B. Behnia, W.G. Buttlar, H. Reis, Characterization of oxidative aging in asphalt concrete – Part 1: ultrasonic velocity and attenuation measurements and acoustic emission response under thermal cooling, Insight 55 (11) (2013) 596–604.
[27] P.A. Johnson, T.J. Shankland, R.J. O'Connell, J.N. Albright, Nonlinear generation of elastic waves in crystalline rock, J. Geophys. Res. 92 (B5) (1987) 3597–3602.
[28] P.A. Johnson, T.J. Shankland, Nonlinear generation of elastic waves in granite and sandstone: continuous wave and travel time observations, J. Geophys. Res. 94 (B12) (1989) 17729–17733.
[29] A.J. Croxford, P.D. Wilcox, B.W. Drinkwater, P.B. Nagy, The use of non-collinear mixing for nonlinear ultrasonic detection of plasticity and fatigue, J. Acoust. Soc. Am. 126 (5) (2009) EL117–EL122.

[30] A. Demcenko, R. Akkerman, P.B. Nagy, R. Loendersloot, Non-collinear wave mixing for nonlinear ultrasonic detection of physical aging in PVC, NDT&E Int. 49 (2012) 34–39.
[31] R.W. Dunham, H.B. Huntington, Ultrasonic beam mixing as a measure of the nonlinear parameters of fused silica and single-crystal NaCl, Phys. Rev. 2 (4) (1970) 1098–1107.
[32] P.B. Nagy, Fatigue damage assessment by nonlinear ultrasonic materials characterization, Ultrasonics 36 (1998) 375–381.
[33] A.F. Braham, W.G. Buttlar, T. Clyne, M. Marasteanu, M. Turos, The effect of long-term laboratory aging on asphalt concrete fracture energy, J. Assoc. Asphalt Paving Technol. 78 (2009) 417–454.